

Multidisciplinary Design Optimization of an Eel-Inspired Soft Robot

Andrew H. Fletcher^{*}, Ru Xiang[†], Jacobo Cervera-Torralba[‡], Michael T. Tolley[§], and John T. Hwang[¶]
University of California, San Diego, La Jolla, CA, 92093

Soft robotic fish have significant potential for underwater applications, with eel-inspired robots offering notable advantages due to the efficiency of their anguilliform swimming motion. This efficiency enables extended range and endurance, making them ideal for various missions. However, designing eel-inspired robots poses significant challenges due to the nonlinear, dynamic fluid-structure interactions (FSI) that drive system performance. Multidisciplinary design optimization (MDO) offers a systematic approach to exploring this unintuitive design space, though few studies have applied MDO to eel-inspired soft robots. While there have been many studies exploring multidisciplinary design optimization with fluid-structure interaction, gradient-based design optimizations with dynamic fluid-structure interaction remains relatively unexplored. A previous study investigated a method for optimizing eel-inspired robots using a static structural model and a dynamic fluids model. While promising, mapping the static structural solution to the dynamic fluids mesh introduces an unquantified amount of modeling error. This study seeks to build on the prior work by investigating the method of directly modeling the dynamic hydroelasticity for shape optimization. Furthermore, this work seeks to demonstrate dynamic hydroelastic shape optimization with analytic unsteady adjoint computation. The method applies a geometry-centric approach, dynamic Euler-Bernoulli beam theory to model structural dynamics, and an unsteady panel method to model the fluid dynamics. Additionally, the models are implemented using a graph-based modeling language to automate the unsteady adjoint computation. The proposed method is applied to optimize the efficiency of an existing modular, eel-inspired soft robot. Furthermore, the method explored in previous work is applied to the same optimization result to investigate the impact of the difference in modeling approach. The presented method shows a 73.9% decrease in cost of transport and 130% increase in swim speed compared to a control optimization of the baseline design. When compared to the optimization result using the static structural model, the optimal designs exhibit similar design trends but significant differences in the scale of the final design. These findings demonstrate the feasibility of automated unsteady hydroelastic adjoint computation and highlight the trade-offs between static and dynamic modeling fidelity in optimizing soft robotic systems.

I. Introduction

SOFT robotic fish offer significant potential for diverse underwater applications, including environmental monitoring [1], deep-sea exploration [2, 3], and aquaculture [4]. Among soft robotic fish concepts, eel-inspired robots are particularly promising due to the efficiency of their anguilliform swimming motion, facilitating longer range and endurance missions [5]. Several prior works have demonstrated eel-inspired robot designs [5–8]. Although there are numerous proposed methods for soft actuation, these studies have investigated using bi-directional fluidic elastomer actuators, which are favored for their ability to generate large forces and achieve rapid bending [9].

Although several prior works have demonstrated eel-inspired designs, designing an effective eel-inspired soft robot remains a challenging task. The underlying physics involves nonlinear, dynamic fluid-structure interactions (FSI), making intuition-driven design impractical. Multidisciplinary design optimization (MDO) offers a systematic method to explore the design space for optimal designs. There have been design optimization studies in soft robotics [10]; however, these studies have typically been restricted to single-discipline models or a limited number of design variables.

^{*}Ph.D. Student, Department of Mechanical and Aerospace Engineering, AIAA Student Member

[†]Ph.D. Student, Department of Mechanical and Aerospace Engineering, AIAA Student Member

[‡]Ph.D. Student, Department of Mechanical and Aerospace Engineering

[§]Professor, Department of Mechanical and Aerospace Engineering

[¶]Assistant Professor, Department of Mechanical and Aerospace Engineering, AIAA Senior Member

While there have been many MDO studies involving FSI, these studies have primarily focused on applications outside of robotics, such as aerospace [11, 12], which differ significantly from the dynamic, large-deformation behavior of soft robotic fish.

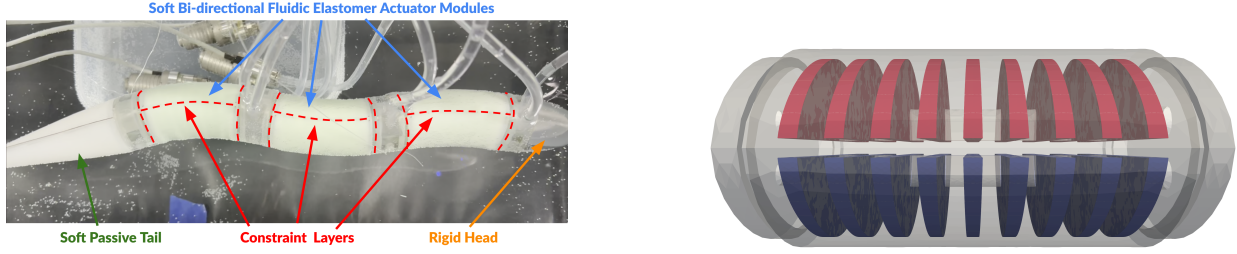
Applying MDO to eel-inspired soft robots presents unique challenges. Unlike steady cases commonly addressed in MDO, anguilliform swimming requires dynamic modeling to capture the periodic system behavior. Furthermore, the hyperelastic materials used in these robots exhibit nonlinear structural dynamics, which are computationally expensive to model. A prior study investigated a method for MDO of an eel-inspired robot using a geometry-centric modeling approach, a static nonlinear finite element structural model, and an unsteady panel method [13]. While promising, the mapping from the static structural solution to the dynamic actuating geometry introduces an unquantified amount of modeling error.

This work seeks to build on this prior study by investigating a method for multidisciplinary, three-dimensional shape optimization of eel-inspired soft robots using a structural dynamics model. In addition, this work demonstrates dynamic hydro-elastic optimization with unsteady adjoint computation. The method combines a dynamic Euler–Bernoulli beam model to capture structural dynamics with an unsteady panel method for fluid dynamics. To ensure consistency in the geometry representation across disciplines, a geometry-centric approach is used for geometry modeling and parameterization. The proposed method is applied to optimize a modular, eel-inspired soft robot consisting of three bi-directional fluidic elastomer actuator modules, a passive soft tail, and a rigid head [6]. In addition, the system is also optimized using an existing method that employs a high-fidelity static structural model and approximates the dynamic actuating geometry. The results of these optimizations are compared, showing a similar design trend but with significantly different cross-section sizes.

II. Background

Design optimization has been explored in soft robotics for diverse applications. Chen and Wang [10] provide a comprehensive review of the methods and applications in the design optimization of soft robots. One prevalent approach is robot evolution, which employs genetic algorithms to optimize designs. Originally applied to rigid robots [14], this approach has since been extended to soft robotics for tasks such as optimizing multi-material walking robots [15], soft pneumatic robots [16], and flexible robotic fish fins [17]. While effective in exploring diverse local optima, robot evolution studies are typically limited to models with rapid evaluation times or a small number of design variables due to the large number of model evaluations evolutionary methods require to explore high-dimensional design spaces. Another popular approach is topology optimization, which has been applied to soft robotic actuators such as cable-driven actuators [18, 19], pneumatic actuators [20, 21], and a magnetic actuator [22]. Topology optimization approaches typically explore a high-dimensional design space; however, the high-dimensional design space often restricts these studies to one or two disciplines with static models.

Shape optimization enables significant design changes while utilizing medium-to-high-fidelity models, making it a promising approach. It has been extensively applied to fluid-structure interaction (FSI) problems using a range of modeling techniques, including panel methods [23], coupled computational fluid dynamics (CFD) and finite element analysis (FEA) models [11], and coupled vortex lattice method (VLM) and spatial beam finite element models [12]. Furthermore, some works have explored dynamic FSI problems with dynamic aeroelasticity [24–26] and dynamic hydroelasticity [27, 28]. However, far fewer studies have investigated dynamic FSI with research typically not yet exploring gradient-based shape optimization. A previous study explored similar modeling approaches for the three-dimensional shape optimization of an eel-inspired soft robot [13]. This method employs a geometry-centric modeling approach, a static three-dimensional nonlinear finite element structural model, and an unsteady panel method for fluid dynamics. Leveraging three-dimensional models enables three-dimensional shape optimization because the model is able to capture the effect of three-dimensional perturbations of the shape. The approach shows significant improvements in the simulated performance of the system and a method for tying the models to the physical system. However, the method introduces unquantified modeling errors by relying on an approximation of the dynamic actuating geometry from a static structural solution. Furthermore, the nonlinear finite element model is computationally expensive and prone to convergence issues with large design changes. This work builds off this prior study by investigating a variation of this approach where the static nonlinear finite element model and corresponding dynamic geometry approximation are replaced with a dynamic Euler-Bernoulli beam model. An Euler-Bernoulli beam model is chosen due to the significant decrease in computational cost needed to model dynamics while maintaining the ability to capture changes in the robot cross-section using a cross-section model. However, the Euler-Bernoulli beam model is unable to capture the nonlinear material properties and detailed geometric properties. This study seeks to investigate the effect of this trade-off between



(a) A top view of the baseline design with the three bi-directional fluidic elastomer actuator modules (blue), the rigid head (orange), and soft passive tail (green). Additionally, the stiff constraint layers are traced (dotted red).

(b) A top view of a bi-directional fluidic elastomer actuator module with the left chambers colored blue, and the right chambers colored red

Fig. 1 The baseline design

dynamic modeling and static modeling fidelity on the optimization results.

This study applies the proposed method to the optimization of an existing modular, eel-inspired soft robot [6]. The design consists of three bi-directional fluidic elastomer actuator modules, a soft passive tail, and a rigid head (Figure 1a). Each actuator produces bending by pumping water between the left and right chambers (Figure 1b). As water is pumped from one side to the other, the inflated side expands, while the opposite side compresses. Fiberglass plates are inserted at the center-line and edges to create the constraint layers. These constraint layers constrain axial deformation and prevent a single side from expanding without creating bending at the center-line.

A. Modeling Overview

The key disciplines in the proposed method include geometry, structural dynamics, and fluid dynamics (Figure 2). First, the optimizer computes the design parameters that are fed to the geometry parameterization model to update the central geometry. The central geometry is then used to compute the beam and cross-sectional meshes for the structural model. The updated meshes and a dynamic input pressure profile are used to simulate the dynamic actuation of the robot and construct the dynamically actuating geometry. The actuating geometry is then used to compute the panel mesh for the unsteady panel solver, which in turn computes the net force on the robot.

III. Modeling Methods

To enable efficient derivative computation, all models are implemented using the Computational System Design Language (CSDL) [29]. CSDL automates the computation of analytic derivatives by constructing a graph representation of the computational model. It traverses this graph in reverse, computing vector-Jacobian products for each operation, and ultimately provides the total derivatives. As such, the computation of the dynamic hydroelastic adjoint is completely automated.

A. Geometry Modeling and Parameterization

The geometry is modeled using a geometry-centric approach, where the central geometry is represented as a single B-spline volume fitted to the CAD model. The mesh nodes for each discipline-specific solver are defined in the parametric space of this B-spline volume. When the control points of the central geometry are adjusted, the meshes are regenerated by reevaluating the B-spline function at the predefined parametric coordinates. This ensures consistency and accuracy of the geometry representation across disciplines with fast evaluation.

The geometry is parameterized using a deformation-based parameterization approach. Free-form deformation (FFD) is used to parameterize the control points of the geometry (Figure 6). The FFD block is represented using an enclosing B-spline volume. To restrict undesirable design changes and reduce the degrees of freedom, the control points of the FFD block are parameterized using a sectional parameterization. The sectional parameterization uses slices of control points of the FFD block to define a series of sections along a principal direction. In this work, four sections are defined normal to the width-direction. Two of these sections enclose the center-line, preventing the optimizer from manipulating

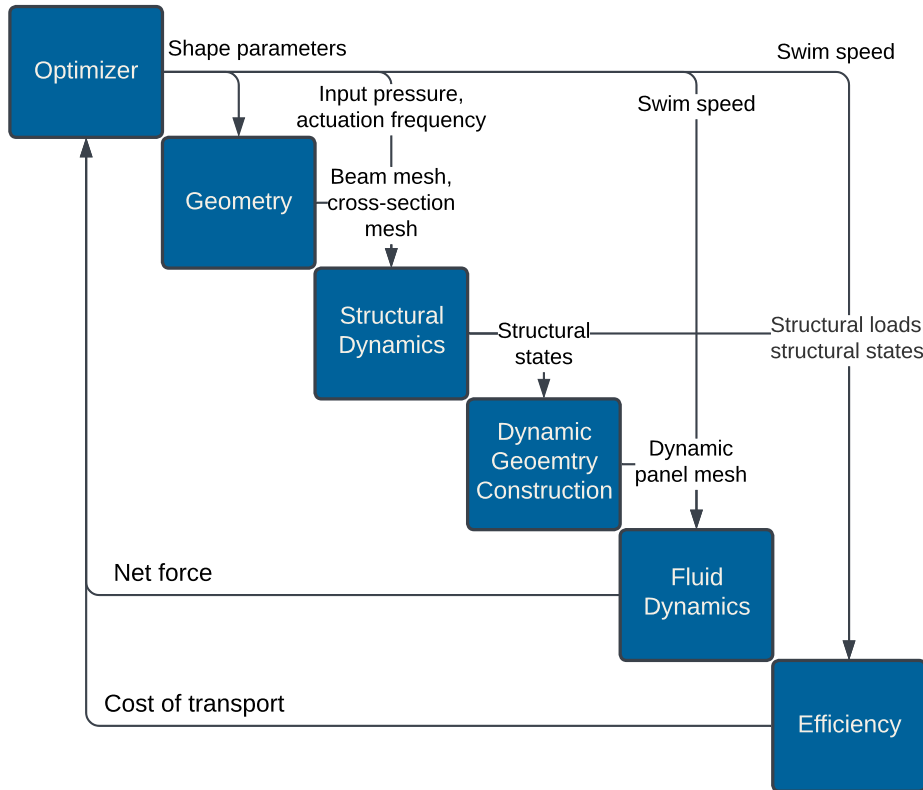
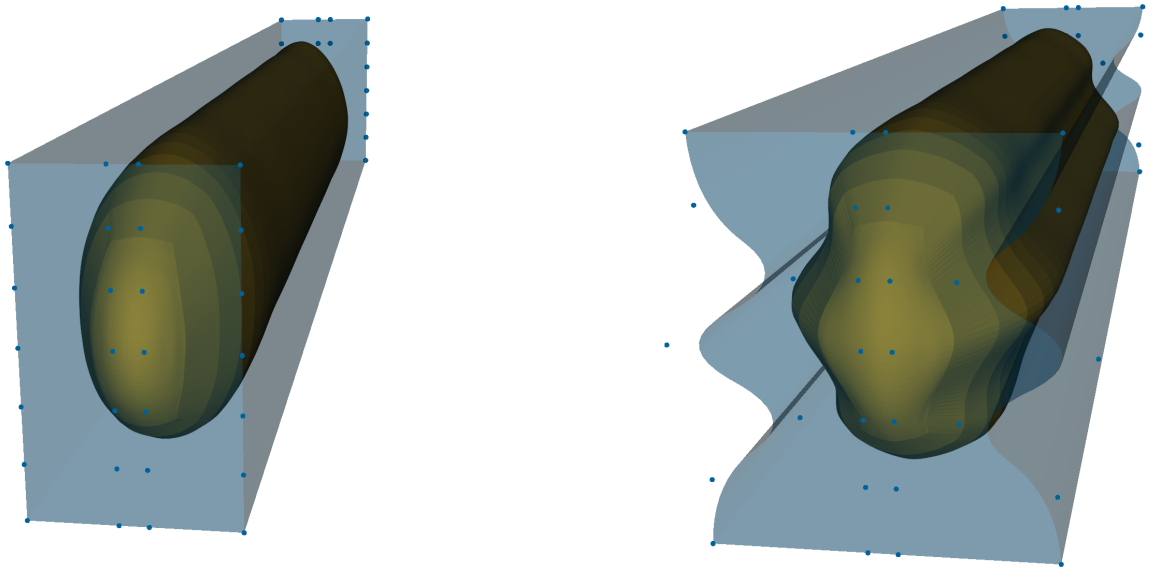


Fig. 2 Model Flowchart



(a) Initial geometry and free-form deformation block

(b) Manipulated geometry and free-form deformation block

Fig. 3 The geometry (gold) and free-form deformation (blue) block for the initial design and for a design with significant changes in the width shape variables and a small change in height. The width shape variables translate the outer control points of the free-form deformation block (blue dots).

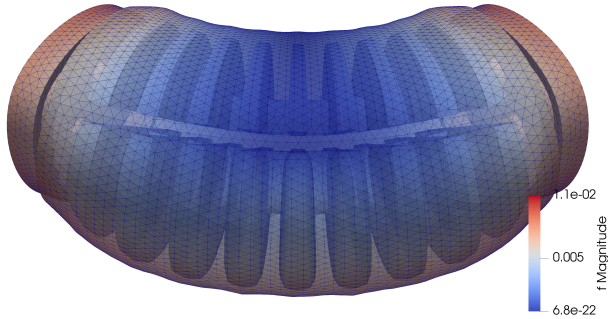


Fig. 4 Static nonlinear finite element solution of the actuation of an actuator module with the baseline design

the thickness of the center-line, which is a design constraint. The other two sections enclose the entire geometry, allowing the optimizer to manipulate the outer cross-section geometry. Finally, a geometry parameterization solver is used to achieve desired high-level design variable values such as robot height and length. To facilitate lower-level design changes, the control points of the FFD block in the outer sections are permitted to move in the width direction. This approach is similar to an approach used for the shape optimization of airfoils [30].

B. Structural Modeling and Dynamic Geometry Construction

The structural model and dynamic geometry construction steps map the input pressure and frequency to the mesh used by the unsteady panel method. While previous work used a static nonlinear finite element approach with simplifying assumptions to approximate the dynamic geometry, this work employs a dynamic Euler-Bernoulli beam model, enabling a more direct mapping from the dynamic states to the dynamic geometry.

1. Static Nonlinear Finite Element Approach

The structural deformation is modeled using a three-dimensional finite element method (FEM) with a nearly-incompressible Neo-Hookean material model (Figure 4). This model is implemented using FEMO [31], which leverages FEniCSx [32, 33] tools for constructing Computational System Design Language (CSDL) models. The finite element mesh is generated with Gmsh [34] and projected into the geometry to compute the parametric coordinates. The states are defined in a continuous Galerkin function space with linear elements. In this work, material parameters are calibrated by minimizing the root-mean-square error (RMSE) between simulated results and experimental measurements of the actuator's bending angle under varying input pressures, resulting in different material parameters from the prior work.

The dynamic geometry is constructed by interpolating the static deformation solution. The maximum deformation profile of an actuator is obtained from the static solution of the actuator. The dynamic geometry is then constructed by linearly interpolating between deformed, undeformed, and mirrored states over time. Using the assumption the input pressure is sinusoidal in time, the interpolation weights are assumed to be sinusoidal in time. To create a traveling wave motion, the actuation profiles of individual actuators are offset in phase equally. Displacement within each actuator is directly applied to the geometry, while the displacement at the front and back edges is propagated rigidly forward and backward, respectively, to the surrounding geometry.

2. Dynamic Beam Approach

The dynamic beam approach employs an Euler-Bernoulli beam model, previously validated for static applications [35] and employed for optimization problems including an urban air mobility (UAM) concept [36] and a power-beaming-enabled aircraft concept [37]. The implementation is extended here to include a dynamic residual formulation, with time integration performed using a generalized-alpha method for energy-conserving and accurate time-stepping [38]. Input loads are applied as equal and opposite moments at the ends of each actuator. The moment is estimated as the product of the chamber pressure, chamber cross-sectional area, and the moment arm, which is computed as the distance between the chamber centroid and the center-line. Input pressures are applied as sinusoidal in time, with equal phase offsets introduced between actuators to produce the traveling wave motion. For each design point, the cross-sectional properties are recomputed from a wire-frame mesh of the cross-section of the central geometry. Additionally, tuning parameters for

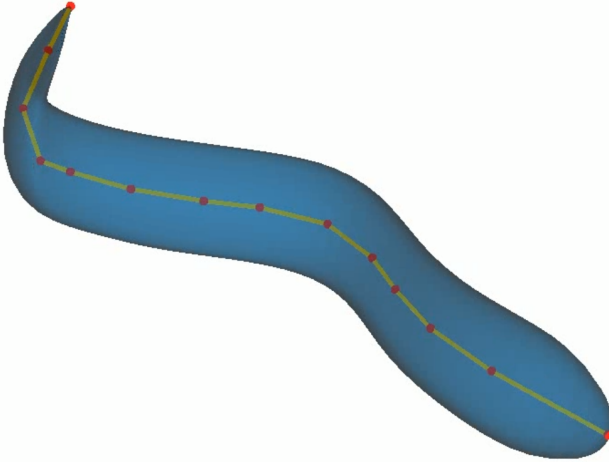


Fig. 5 Dynamic geometry (blue) computed from the dynamic beam states. The deformed beam mesh is overlaid (yellow with red dots at the nodes).

input pressure, damping, and material densities are inserted and calibrated to match experimental behavior. To enforce periodicity of the solution, fixed-point iteration is used to enforce that the degrees of freedom of the beam, as well as their velocities and accelerations, are equal at the initial and final time steps.

The dynamic geometry is computed as an affine mapping from the beam states. During the setup phase, a piecewise-linear function is fitted to the beam mesh, and a wire-frame representation of the geometry is projected onto this function. At each time step, wire-frame points are assigned displacements corresponding to their projected positions along the beam solution. The resulting wire-frame displacements are used to fit a displacement function in the same function space as the geometry. The dynamic geometry is then computed by adding the displacement function with the undeformed geometry function at each time step (Figure 5).

C. External Hydrodynamics Modeling

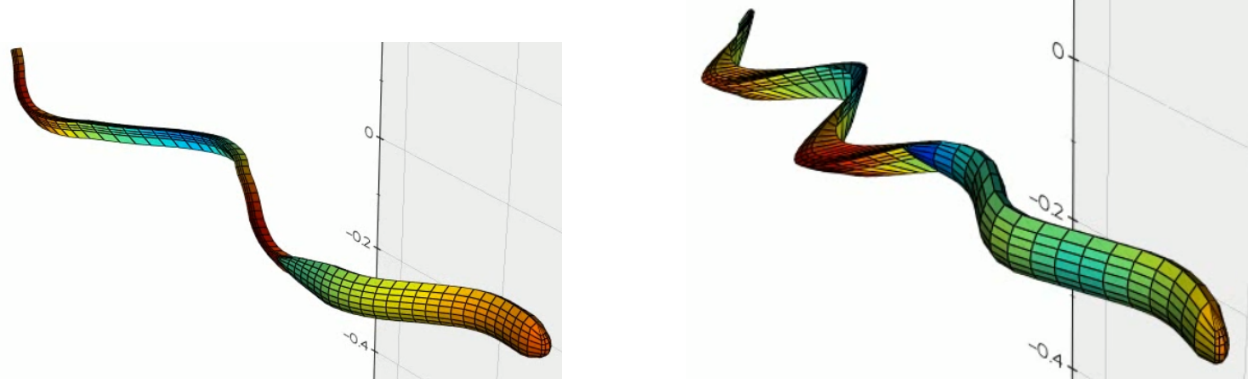
The external fluid dynamics are modeled using an unsteady panel method combined with a boundary layer model and a prescribed wake. To improve the accuracy of the solution, the unsteady panel method is run for two periods. The first period is used to build up the wake, and the second period is used to compute the model outputs. By using an unsteady panel method rather than a vortex lattice method or lower-fidelity model, the solver captures the effects of perturbations in the thickness of the geometry. By using a vortex-based method rather than a computational fluid dynamics (CFD) method, the dynamics can be captured robustly with significantly lower computational cost.

D. Efficiency Modeling

System efficiency is evaluated using an approximate cost of transport (CoT) metric, defined as the input power divided by swimming speed. This metric quantifies the energy cost to travel one meter, serving as an effective metric for efficiency. With the static nonlinear finite element approach, which lacks a dynamic model, input power is approximated using a surrogate metric. Specifically, the mechanical work done on the static structure is divided by the actuation period to compute the input power. This surrogate metric has units of power and scales proportionally, leading to an equivalent optimal solution, but does not measure the true cost of transport. With the dynamic beam method, the input average power is computed by integrating the power over time and dividing by the total time. These objective formulations produce equivalent optimal solutions, but the different formulations make it difficult to compare the quantities directly.

IV. Optimization Results

The optimization problem is formulated to minimize the cost of transport (CoT) while satisfying a trim constraint (Table 1). To ensure operational effectiveness, a swimming speed of 0.66 body lengths per second is prescribed. The robot's cross-sectional geometry is parameterized using four width variables and one height variable, enabling optimization of the shape. Double symmetry is enforced, mirroring the shape changes to reduce the number of design



(a) Static nonlinear finite element method

(b) Dynamic beam method

Fig. 6 A snapshot of the dynamic geometry and corresponding unsteady panel solution is shown for the static nonlinear finite element method and the proposed dynamic beam method. The color represents the doublet strength in the unsteady panel method solution.

	Variable	Lower Bound	Upper Bound
Objective	Cost of transport		
Design Variables	Actuation frequency	0.5 Hz	2 Hz
	Maximum pump pressure	5 kPa	37.5 kPa
	Width shape variables (x4)	-40%	+100%
	Height	4 cm	13.35 cm
Constraint	Net force = 0		

Table 1 Optimization Problem Formulation

variables. Additionally, actuation frequency and maximum pressure were included as optimization variables, allowing the optimization to identify an optimal combination of design and control parameters rather than being constrained to a fixed control setup.

The optimization problem is solved for both the static nonlinear method and the dynamic beam method using the PySLSQP optimizer [39, 40] within the modOpt environment [41]. The static nonlinear finite element model resulted in a cross-sectional shape with significantly wider top and bottom sections and a thicker middle. However, the width at the third control point, located above the center-line, decreased sharply. For the dynamic beam method, the optimal solution has a slightly wider top and bottom, a significantly thinner middle, and a noticeably shorter overall height (Figure 7). Interestingly, while the two middle control points reduced the width to their lower bounds, the bottom control point, located at the center of the cross-section, remained above its minimum. As such, the optimized result using the dynamic beam method showed a 73.9% reduction in the simulated cost of transport and 130% increase in speed compared to baseline control optimization without design changes (Table 2). The control optimization problem uses a prescribed swim speed of 0.13 m/s because the optimizer did not converge for a prescribed swim speed of 0.3 m/s and 0.13 m/s is the swim speed experimentally found to satisfy trim for the baseline design with manually prescribed controls [13, 42].

V. Discussion

The two modeling approaches produce distinct optimal geometries, although both designs suggest elements of a shared underlying design concept. The optimization using the dynamic beam method resulted in a cross-section that was significantly thinner and shorter than that produced by the static nonlinear finite element method. Despite these differences, both designs exhibited a consistent trend: starting from the top of the cross-section, the width initially increases, then decreases near the middle, and subsequently increases again at the lower control points. This pattern suggests that both methods may potentially be exploiting similar physical principles to optimize the geometry, with an exception in the absolute scale of the cross-section. During the material parameter tuning process, it was observed

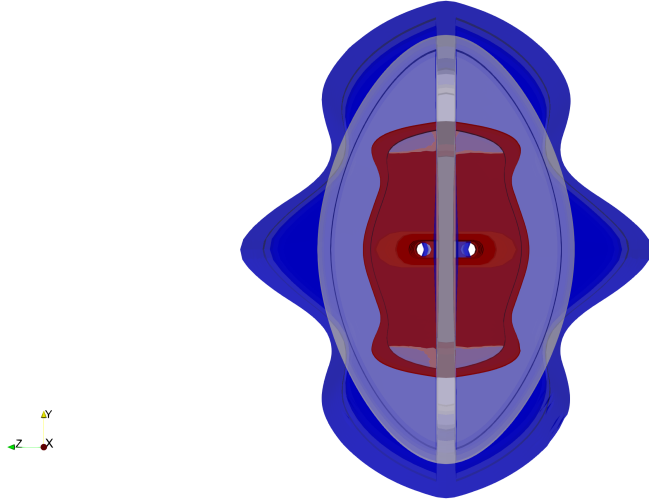


Fig. 7 An overlay of the cross-sections of the baseline design (gray), optimization result using static nonlinear modeling method (blue), and optimization result using the dynamic beam modeling method (red)

	Baseline Design with Opt. Control	Dynamic Method	Static Method
Cost of transport	37.2 J/m	9.7 J/m	-
Swim speed	0.13 m/s	0.3 m/s	0.3 m/s
Actuation frequency	0.766 Hz	0.767 Hz	0.360 Hz
Maximum pump pressure	22.6 kPa	29.8 kPa	22.4 kPa
Width shape variable 1	0%	+86%	+65%
Width shape variable 2	0%	-40%	+62%
Width shape variable 3	0%	-40%	-30%
Width shape variable 4	0%	-34%	+98%
Height	6.7 cm	4.0 cm	7.7 cm

Table 2 Optimization Results

that increasing the stiffness of the fiberglass constraint layer relative to the soft silicone material decreased bending more for actuators with thinner cross-sections. With softer silicone, increasing the cross-section thickness did not significantly enhance stiffness but did increase torque, leading to more bending in thicker designs. Considering that the static nonlinear finite element model is calibrated using experimental data, the discrepancy in thickness of the designs seems to imply that the dynamic beam model may have modeling error in the relative stiffness contributions of the soft silicone and stiff constraint layers. On the other hand, a noticeable observation through the optimization process is that there are many local optima in the design space. The prevalence of these local optima can lead to significantly different optimized designs with even small changes to the initial conditions or modeling. This study attempted to run the optimizations for a variety of initial conditions in an attempt to find the global optimum, but it is possible that the difference in the modeling approaches led the optimizers to converge to unique local optima.

In addition to the optimization results, the development and implementation of the dynamic beam method provided insights into the design process. One key observation was the sensitivity of thrust generation to the phase behavior of the actuators. If the back actuator fell out of phase with the others, thrust generation became nearly impossible. The unsteady panel method solution showed that instead of propagating the pressure wave toward the tail as intended, the wave reversed direction at the back actuator and propagated toward the head. This behavior highlights the importance of ensuring proper wave propagation for effective propulsion and demonstrates the dynamic method's capability to identify such critical performance issues during the design process.

VI. Conclusion

This study presented and investigated a multidisciplinary design optimization method for optimizing eel-inspired soft robots. The method used a dynamic Euler-Bernoulli beam model and featured a fully automated computation of the dynamic hydroelastic adjoint. The proposed method demonstrated a 73.9% simulated decrease in the cost of transport. In addition, the optimization problem is solved again using a previously presented method featuring a static nonlinear structural modeling approach, and the optimization results of the two methods are compared. While both methods revealed similar trends in the optimized geometry, the dynamic method produced a design with a significantly thinner and shorter cross-section.

While the presented method showed a significant increase in design performance, discrepancies between the optimal designs obtained from the two approaches raise questions about the underlying causes. These differences may result from modeling errors in one or both approaches, or from the optimizer simply converging to different local optima. These uncertainties highlight the need for further validation of the modeling techniques. Future research could prioritize validating and tuning the fully dynamic hydroelastic approach through rigorous comparisons of simulated results with experimental data to increase confidence in the dynamic modeling framework. Another promising avenue includes combining the dynamic and static methods, such as incorporating a dynamic nonlinear finite element model or using static nonlinear finite element solutions to calibrate the dynamic beam model. In addition, manufacturing and experimentally testing optimized designs would enable quantification of the accuracy of the full system model and the real-world effect on system performance.

Acknowledgments

This work was supported, in part, by the Office of Naval Research, grant number N00014-22-1-2595.

References

- [1] Katschmann, R. K., DelPreto, J., MacCurdy, R., and Rus, D., “Exploration of underwater life with an acoustically controlled soft robotic fish,” *Science Robotics*, Vol. 3, No. 16, 2018, p. eaar3449. <https://doi.org/10.1126/scirobotics.aar3449>, URL <https://www.science.org/doi/abs/10.1126/scirobotics.aar3449>.
- [2] Li, G., Wong, T.-W., Shih, B., Guo, C., Wang, L., Liu, J., Wang, T., Liu, X., Yan, J., Wu, B., Yu, F., Chen, Y., Liang, Y., Xue, Y., Wang, C., He, S., Wen, L., Tolley, M., Zhang, A.-M., and Li, T., “Bioinspired soft robots for deep-sea exploration,” *Nature Communications*, Vol. 14, 2023. <https://doi.org/10.1038/s41467-023-42882-3>.
- [3] Li, G., Chen, X., Zhou, F., Liang, Y., Xiao, Y., Xunuo, C., Zhang, Z., Zhang, M., Wu, B., Yin, S., Xu, Y., Fan, H., Chen, Z., Song, W., Yang, W., Pan, B., Hou, J., Zou, W., He, S., and Yang, W., “Self-powered soft robot in the Mariana Trench,” *Nature*, Vol. 591, 2021, pp. 66–71. <https://doi.org/10.1038/s41586-020-03153-z>.
- [4] Li, G., Deng, Y., Osen, O. L., Bi, S., and Zhang, H., “A bio-inspired swimming robot for marine aquaculture applications: From concept-design to simulation,” *OCEANS 2016 - Shanghai*, 2016, pp. 1–7. <https://doi.org/10.1109/OCEANSAP.2016.7485691>.
- [5] Nguyen, D. Q., and Ho, V. A., “Anguilliform Swimming Performance of an Eel-Inspired Soft Robot,” *Soft Robotics*, Vol. 9, No. 3, 2022, pp. 425–439. <https://doi.org/10.1089/soro.2020.0093>, URL <https://doi.org/10.1089/soro.2020.0093>, pMID: 34134542.
- [6] Cervera-Torralba, J., Kang, Y., Khan, E. M., Adibnazari, I., and Tolley, M. T., “Lost-Core Injection Molding of Fluidic Elastomer Actuators for the Fabrication of a Modular Eel-Inspired Soft Robot,” *2024 IEEE 7th International Conference on Soft Robotics (RoboSoft)*, 2024, pp. 971–976. <https://doi.org/10.1109/RoboSoft60065.2024.10522050>.
- [7] Feng, H., Sun, Y., Todd, P. A., and Lee, H. P., “Body Wave Generation for Anguilliform Locomotion Using a Fiber-Reinforced Soft Fluidic Elastomer Actuator Array Toward the Development of the Eel-Inspired Underwater Soft Robot,” *Soft Robotics*, Vol. 7, No. 2, 2020, pp. 233–250. <https://doi.org/10.1089/soro.2019.0054>, URL <https://doi.org/10.1089/soro.2019.0054>, pMID: 31851869.
- [8] Chen, Y., Wang, T., Wu, C., and Wang, X., “Design, control, and experiments of a fluidic soft robotic eel,” *Smart Materials and Structures*, Vol. 30, No. 6, 2021, p. 065001. <https://doi.org/10.1088/1361-665X/abf5ef>, URL <https://dx.doi.org/10.1088/1361-665X/abf5ef>.
- [9] Pagoli, A., Chapelle, F., Corrales-Ramon, J.-A., Mezouar, Y., and Lapusta, Y., “Review of soft fluidic actuators: classification and materials modeling analysis,” *Smart Materials and Structures*, Vol. 31, No. 1, 2021, p. 013001. <https://doi.org/10.1088/1361-665X/ac383a>, URL <https://dx.doi.org/10.1088/1361-665X/ac383a>.

- [10] Chen, F., and Wang, M. Y., "Design Optimization of Soft Robots: A Review of the State of the Art," *IEEE Robotics Automation Magazine*, Vol. 27, No. 4, 2020, pp. 27–43. <https://doi.org/10.1109/MRA.2020.3024280>.
- [11] Kenway, G., Kennedy, G., and Martins, J. R. R. A., *A CAD-Free Approach to High-Fidelity Aerostructural Optimization*, 2012. <https://doi.org/10.2514/6.2010-9231>, URL <https://arc.aiaa.org/doi/abs/10.2514/6.2010-9231>.
- [12] Jasa, J., Hwang, J., and Martins, J., "Open-source coupled aerostructural optimization using Python," *Structural and Multidisciplinary Optimization*, Vol. 57, 2018. <https://doi.org/10.1007/s00158-018-1912-8>.
- [13] Fletcher, A. H., Xiang, R., Scotzniovsky, L., Cervera-Torralba, J., Tolley, M. T., and Hwang, J. T., "Multidisciplinary Control Co-Design Optimization of Anguilliform-Swimming Soft Fluidic Robots," , 2025. Submitted for publication.
- [14] Sims, K., "Evolving 3D Morphology and Behavior by Competition," *Artificial Life*, Vol. 1, No. 4, 1994, pp. 353–372. <https://doi.org/10.1162/artl.1994.1.4.353>, URL <https://doi.org/10.1162/artl.1994.1.4.353>.
- [15] Cheney, N., MacCurdy, R., Clune, J., and Lipson, H., "Unshackling Evolution: Evolving Soft Robots with Multiple Materials and a Powerful Generative Encoding," 2013. <https://doi.org/10.1145/2463372.2463404>.
- [16] Bodily, D. M., Allen, T. F., and Killpack, M. D., "Multi-objective design optimization of a soft, pneumatic robot," *2017 IEEE International Conference on Robotics and Automation (ICRA)*, 2017, pp. 1864–1871. <https://doi.org/10.1109/ICRA.2017.7989218>.
- [17] Clark, A. J., Tan, X., and McKinley, P. K., "Evolutionary multiobjective design of a flexible caudal fin for robotic fish," *Bioinspiration Biomimetics*, Vol. 10, No. 6, 2015, p. 065006. <https://doi.org/10.1088/1748-3190/10/6/065006>, URL <https://dx.doi.org/10.1088/1748-3190/10/6/065006>.
- [18] Chen, F., Xu, W., Zhang, H., Wang, Y., Cao, J., Wang, M. Y., Ren, H., Zhu, J., and Zhang, Y. F., "Topology Optimized Design, Fabrication, and Characterization of a Soft Cable-Driven Gripper," *IEEE Robotics and Automation Letters*, Vol. 3, No. 3, 2018, pp. 2463–2470. <https://doi.org/10.1109/LRA.2018.2800115>.
- [19] Liu, Y., and Wang, M. Y., "Topology design of a conforming gripper with distributed compliance via a level set method," *2014 IEEE International Conference on Robotics and Biomimetics (ROBIO 2014)*, 2014, pp. 2191–2196. <https://doi.org/10.1109/ROBIO.2014.7090662>.
- [20] Zhang, H., Wang, M. Y., Chen, F., Wang, Y., Kumar, A. S., and Fuh, J. Y. H., "Design and development of a soft gripper with topology optimization," *2017 IEEE/RSJ International Conference on Intelligent Robots and Systems (IROS)*, 2017, pp. 6239–6244. <https://doi.org/10.1109/IROS.2017.8206527>.
- [21] Chen, Y., Xia, Z., and Zhao, Q., "Optimal Design of Soft Pneumatic Bending Actuators Subjected to Design-Dependent Pressure Loads," *IEEE/ASME Transactions on Mechatronics*, Vol. 24, No. 6, 2019, pp. 2873–2884. <https://doi.org/10.1109/TMECH.2019.2943418>.
- [22] Tian, J., Zhao, X., Gu, X. D., and Chen, S., "Designing Ferromagnetic Soft Robots (FerroSoRo) with Level-Set-Based Multiphysics Topology Optimization," *2020 IEEE International Conference on Robotics and Automation (ICRA)*, 2020, pp. 10067–10074. <https://doi.org/10.1109/ICRA40945.2020.9197457>.
- [23] Conlan-Smith, C., Ramos-García, N., Sigmund, O., and Andreasen, C. S., "Aerodynamic Shape Optimization of Aircraft Wings Using Panel Methods," *AIAA Journal*, Vol. 58, No. 9, 2020, pp. 3765–3776. <https://doi.org/10.2514/1.J058979>, URL <https://doi.org/10.2514/1.J058979>.
- [24] Parsons, W. P., Gasparetto, V. E. L., ElSayed, M. S. A., Saad, M., Shield, S., Brown, G. L., and Hilliard, L. M., "Dynamic Aeroelastic Performance Optimization of Adaptive Aerospace Structures Using Structural Geometric Nonlinearities," *Journal of Aerospace Engineering*, Vol. 35, No. 6, 2022, p. 04022089. [https://doi.org/10.1061/\(ASCE\)AS.1943-5525.0001465](https://doi.org/10.1061/(ASCE)AS.1943-5525.0001465), URL <https://ascelibrary.org/doi/abs/10.1061/%28ASCE%29AS.1943-5525.0001465>.
- [25] Saporito, M., Da Ronch, A., Bartoli, N., and Defoort, S., "Robust multidisciplinary analysis and optimization for conceptual design of flexible aircraft under dynamic aeroelastic constraints," *Aerospace Science and Technology*, Vol. 138, 2023, p. 108349. <https://doi.org/https://doi.org/10.1016/j.ast.2023.108349>, URL <https://www.sciencedirect.com/science/article/pii/S1270963823002468>.
- [26] Werter, N., and De Breuker, R., "A novel dynamic aeroelastic framework for aeroelastic tailoring and structural optimisation," *Composite Structures*, Vol. 158, 2016, pp. 369–386. <https://doi.org/https://doi.org/10.1016/j.compstruct.2016.09.044>, URL <https://www.sciencedirect.com/science/article/pii/S0263822316318669>.

- [27] Ng, G. W., Martins, J. R., and Young, Y. L., “Optimizing steady and dynamic hydroelastic performance of composite foils with low-order models,” *Composite Structures*, Vol. 301, 2022, p. 116101. <https://doi.org/https://doi.org/10.1016/j.compstruct.2022.116101>, URL <https://www.sciencedirect.com/science/article/pii/S02638223200839X>.
- [28] Ng, G. W., Jonsson, E., He, S., and Martins, J. R., “Dynamic hydroelasticity of composite appendages with reverse-mode algorithmic differentiation,” *Composite Structures*, Vol. 346, 2024, p. 118367. <https://doi.org/https://doi.org/10.1016/j.compstruct.2024.118367>, URL <https://www.sciencedirect.com/science/article/pii/S0263822324004951>.
- [29] Gendarillas, V., Joshy, A. J., Sperry, M., Ivanov, A., and Hwang, J., “A graph-based methodology for constructing computational models that automates adjoint-based sensitivity analysis,” *Structural and Multidisciplinary Optimization*, Vol. 67, 2024. <https://doi.org/10.1007/s00158-024-03792-0>.
- [30] He, X., Li, J., Mader, C. A., Yildirim, A., and Martins, J. R., “Robust aerodynamic shape optimization—From a circle to an airfoil,” *Aerospace Science and Technology*, Vol. 87, 2019, pp. 48–61. <https://doi.org/https://doi.org/10.1016/j.ast.2019.01.051>, URL <https://www.sciencedirect.com/science/article/pii/S1270963818319072>.
- [31] Xiang, R., van Schie, S., Scotzniovsky, L., Yan, J., Kamensky, D., and Hwang, J., “Automating adjoint sensitivity analysis for multidisciplinary models involving partial differential equations,” , 07 2024. <https://doi.org/10.21203/rs.3.rs-4265983/v1>.
- [32] Baratta, I. A., Dean, J. P., Dokken, J. S., Habera, M., Hale, J. S., Richardson, C. N., Rognes, M. E., Scroggs, M. W., Sime, N., and Wells, G. N., “DOLFINx: The next generation FEniCS problem solving environment,” , Dec. 2023. <https://doi.org/10.5281/zenodo.10447666>, URL <https://doi.org/10.5281/zenodo.10447666>.
- [33] Alnæs, M. S., Logg, A., Ølgaard, K. B., Rognes, M. E., and Wells, G. N., “Unified form language: A domain-specific language for weak formulations of partial differential equations,” *ACM Trans. Math. Softw.*, Vol. 40, No. 2, 2014. <https://doi.org/10.1145/2566630>, URL <https://doi.org/10.1145/2566630>.
- [34] Geuzaine, C., and Remacle, J.-F., “Gmsh: A 3-D finite element mesh generator with built-in pre-and post-processing facilities,” *International journal for numerical methods in engineering*, Vol. 79, No. 11, 2009, pp. 1309–1331.
- [35] Sarojini, D., Ruh, M., Yan, J., Scotzniovsky, L., Orndorff, N. C., Xiang, R., Zhao, H., Krokowski, J., Warner, M., van Schie, S., Cronk, A., Guibert, A. T., Chambers, J. T., Wolfe, L., Doring, R., Despins, R., Joseph, C., Anderson, R., Ning, A., Gill, H., Lee, S., Cheng, Z., Cao, Z., Mi, C., Meng, Y. S., Silva, C., Chen, J.-S., Kim, A. A., and Hwang, J. T., *Review of Computational Models for Large-Scale MDAO of Urban Air Mobility Concepts*, 2024. <https://doi.org/10.2514/6.2024-0377>, URL <https://arc.aiaa.org/doi/abs/10.2514/6.2024-0377>.
- [36] Ruh, M. L., Fletcher, A., Sarojini, D., Sperry, M., Yan, J., Scotzniovsky, L., van Schie, S. P., Warner, M., Orndorff, N. C., Xiang, R., Joshy, A. J., Zhao, H., Krokowski, J., Gill, H., Lee, S., Cheng, Z., Cao, Z., Mi, C., Silva, C., Wolfe, L., Chen, J.-S., and Hwang, J. T., *Large-scale multidisciplinary design optimization of a NASA air taxi concept using a comprehensive physics-based system model*, 2024. <https://doi.org/10.2514/6.2024-0771>, URL <https://arc.aiaa.org/doi/abs/10.2514/6.2024-0771>.
- [37] Orndorff, N. C., Wang, B., Ruh, M. L., Fletcher, A., and Hwang, J. T., *Gradient-based sizing optimization of power-beaming-enabled aircraft*, 2023. <https://doi.org/10.2514/6.2023-4019>, URL <https://arc.aiaa.org/doi/abs/10.2514/6.2023-4019>.
- [38] Chung, J., and Hulbert, G. M., “A Time Integration Algorithm for Structural Dynamics With Improved Numerical Dissipation: The Generalized- Method,” *Journal of Applied Mechanics*, Vol. 60, No. 2, 1993, pp. 371–375. <https://doi.org/10.1115/1.2900803>, URL <https://doi.org/10.1115/1.2900803>.
- [39] Joshy, A. J., and Hwang, J. T., “PySLSQP: A transparent Python package for the SLSQP optimization algorithm modernized with utilities for visualization and post-processing,” *arXiv preprint arXiv:2408.13420*, 2024. <https://doi.org/10.48550/arXiv.2408.13420>.
- [40] Kraft, D., “A software package for sequential quadratic programming,” *Forschungsbericht- Deutsche Forschungs- und Versuchsanstalt fur Luft- und Raumfahrt*, 1988.
- [41] Joshy, A. J., and Hwang, J. T., “modOpt: A modular development environment and library for optimization algorithms,” *arXiv preprint arXiv:2410.12942*, 2024. <https://doi.org/10.48550/arXiv.2410.12942>.
- [42] Park, M., Cervera-Torralba, J., Adibnazari, I., and Tolley, M. T., “Analysis on kinematics and propulsion of a self-sensing multi-DoF undulating robotic fish,” , 2025. Submitted for publication.